Phonon origin and lattice evolution in charge density wave states

Heather M. Hill,[1] Sugata Chowdhury,[1] Jeffrey R. Simpson,[1,2] Albert F. Rigosi,[1] David B. Newell,[1] Helmuth Berger,[3] Francesca Tavazza,[1] and Angela R. Hight Walker[1,*]

[1]*National Institute of Standards and Technology (NIST), Gaithersburg, Maryland 20899, USA*

[2]*Towson University, Towson, Maryland 21252, USA*

[3]*École Polytechnique Fédérale de Lausanne (EPFL), Institut de Physique des Nanostructures, CH-1015 Lausanne, Switzerland*

(Received 20 March 2019; published 20 May 2019)

Metallic transition metal dichalcogenides, such as tantalum diselenide ($TaSe_2$), display quantum correlated phenomena of superconductivity and charge density waves (CDWs) at low temperatures. Here, the photophysics of 2H-$TaSe_2$ during CDW transitions is revealed by combining temperature-dependent, low-frequency Raman spectroscopy and density functional theory (DFT). The spectra contain amplitude, phase, and zone-folded modes that are assigned to specific phonons and lattice restructuring predicted by DFT calculations with superb agreement. The noninvasive and efficient optical methodology detailed here demonstrates an essential link between atomic-scale and microscopic quantum phenomena.

DOI: 10.1103/PhysRevB.99.174110

I. INTRODUCTION

A charge density wave (CDW) is a quantum phenomenon in correlated systems [1–8], and in addition to being of enormous theoretical interest, CDW states show promise as a switchable state for tuning electrical properties in device applications [1]. The CDW state is a periodic distortion of the atomic position and a corresponding modulation of the electron density that occurs below a critical transition temperature [2]. CDW periodicity may be an integer multiple of the undistorted lattice constant (commensurate) or an unrelated periodicity (incommensurate). Accompanying this change in lattice periodicity is a localized band splitting at the Fermi level that lowers the overall energy of the system. At low temperature, many metallic TMDs also display superconductivity, which competes with CDW states [4,5]. CDW formation in metallic TMDs has been theorized to emerge from several coexisting mechanisms such as Fermi surface nesting [9], saddle-point singularities [10], and electron-phonon interactions [3,11–14]. However, knowledge of the cause of CDW formation does not provide information regarding the structural transition as the CDW forms. In particular, the details of the evolution of atomic structure associated with the lattice distortion and its effects on the phonon modes have not been correlated.

A prototype for studying CDW formation is 2H tantalum diselenide ($TaSe_2$), whose atomic layered structure is shown in Fig. 1 (inset). Bulk 2H-$TaSe_2$ exhibits an incommensurate CDW phase below 122 K and a commensurate CDW phase below 90 K [15,16]. CDW formation in 2H-$TaSe_2$ is one of the most studied, yet debated, topics for this material [7,15–23]. There is much disagreement as to the assignment of the four, low-frequency (LF) Raman modes [7], given that, in a one-dimensional chain model, the CDW is expected to have only one Raman-active amplitude mode [2]. Holy *et al.* argued that the threefold degeneracy of the phase and amplitude modes, expected for a three-dimensional (3D) material, should be lifted due to symmetry [17]. It then follows that two of the peaks would emerge as phase modes and the other two as amplitude modes. Alternatively, the additional features could arise due to carriers coupling to multiple phonon bands [6], or they could result from multiple or coupled order parameters in the free energy of the CDW state [16]. A consensus regarding the assignment of the LF peaks and the microscopic detail of the atomic structures associated with these modes has not been reached. Furthermore, no discussion of the other midfrequency peaks that are only observed in the CDW state has occurred. Given the promising properties of $TaSe_2$, such as predicted strain-induced ferromagnetism in monolayers and demonstrated functionality in switches and logic circuits [24,25], and the technological applications of CDW states more broadly, it is crucial to correlate the atomic displacements with a noninvasive, facile optical method.

Low-temperature and LF Raman spectroscopy are combined with density functional theory (DFT) to unveil lattice distortion and vibrations associated with CDW states, which are accompanied by a small localized band splitting at the Fermi level on the order of 5 meV. Specifically, we identify how the modes change as a function of temperature as the transition to the CDW states occurs. These Raman experiments greatly improve and expand upon the information presented in early works [6–8], and some enhancements, such as higher spectral resolution and more refined temperature steps, allow us to distinguish the unique behavior of the LF CDW modes, midfrequency CDW modes, and Raman phonon modes seen in both the undistorted and distorted states. Using similar temperature increments for our DFT calculations, in the form of an electronic temperature, we model the behavior of all of the aforementioned Raman modes. With this thorough comparison of DFT to experiment, definitive assignments of the origin of the experimental modes are made to corresponding lattice restructuring and vibrations observable optically.

*Corresponding author: angela.hightwalker@nist.gov

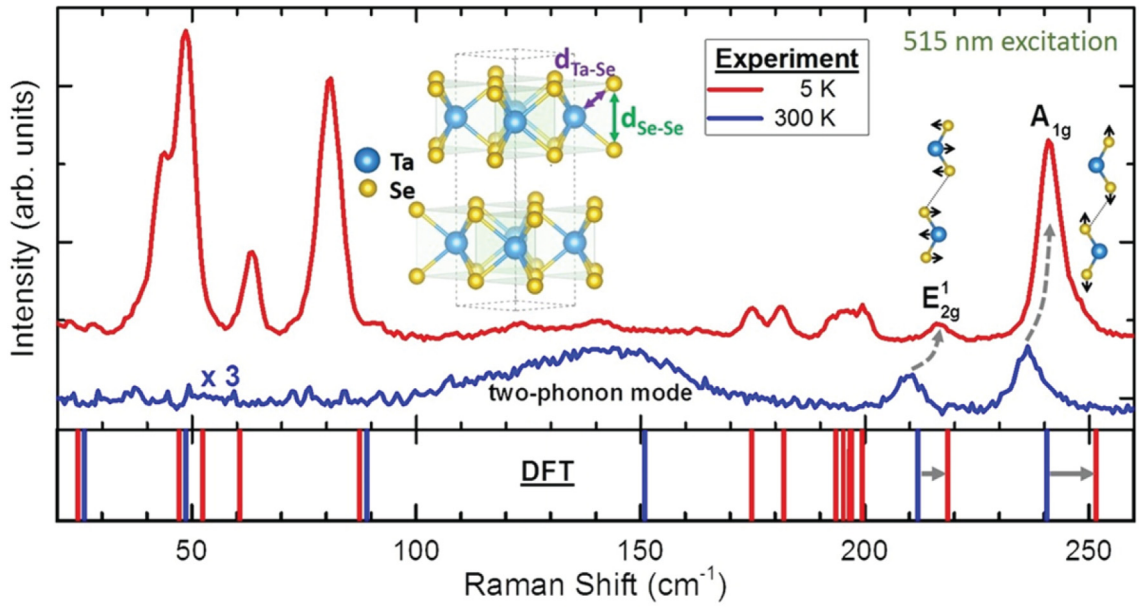

FIG. 1. (Top) 300 K (blue curve) and 5 K (red curve) Raman spectrum of $TaSe_2$ ($\lambda = 515$ nm). The 300 K spectrum (multiplied by a factor of 3 for clarity) consists of three modes: the two-phonon mode at 151 cm^{-1}, the E^1_{2g} mode at 212 cm^{-1}, and the A_{1g} mode at 241 cm^{-1}. The vibrations are shown schematically from a side view of the lattice. The 5 K spectrum consists of the E^1_{2g} and A_{1g} modes, as well as additional modes due to the CDW, most notably the intense peaks below 100 cm^{-1} and several midfrequency peaks between 175 cm^{-1} and 200 cm^{-1}. (Bottom) DFT-calculated Raman mode frequencies for electronic temperatures of 10 K (red lines) and 300 K (blue lines). The gray arrows indicate that the 10 and 300 K lines are the same mode.

II. EXPERIMENTAL AND THEORETICAL METHODS

Mechanically exfoliated, single crystals of 2H-$TaSe_2$ on Si/SiO_2 substrates (300-nm oxide layer) are shown in the optical micrograph in Fig. 1-SM of the Supplemental Material (SM) [26] (also see [27–36]). Temperature-dependent Raman spectra were collected from 5 to 300 K using both 633- and 515-nm laser excitation [26] while the sample is in a cryostat. The inelastically scattered light was collected through a triple-grating spectrometer to enable LF (down to approximately 10 cm^{-1}) Raman measurements. DFT calculations were completed using the open source QUANTUM ESPRESSO (QE) package [37]. While the DFT calculations were performed at 0 K, the temperature effects behind the formation of the CDW states were modeled by tuning the smearing factor, σ, which describes the Fermi-Dirac distribution [32,34]. Further details are provided in the SM [26].

III. EXPERIMENTAL AND THEORETICAL RESULTS

A. Temperature-dependent mode behavior

In Fig. 1 Raman spectra at 5 and 300 K are shown for 2H-$TaSe_2$ with the DFT-calculated Raman modes. The experimental spectra were collected from a diffraction-limited spot using 0.5 mW of 515-nm excitation. The DFT modes were calculated using a $(3 \times 3 \times 1)$ superlattice at two different electronic temperatures, 10 and 300 K. Three Raman modes are experimentally observed in bulk 2H-$TaSe_2$ at room temperature (300 K): a two-phonon mode, E^1_{2g}, and A_{1g}. The broad two-phonon mode around 150 cm^{-1} is a second-order scattering of two modes associated with the Kohn anomaly with opposite wave vectors and depends on the interband phonon resonance of d electrons [6,38,39]. This two-phonon mode is closely related to the size and shape of the phonon anomaly and, in some simpler cases like this one, the two quantities can be approximated as being indirectly proportional to one another. The E^1_{2g} is an in-plane vibration of the selenium and tantalum atoms in opposite directions, whereas the A_{1g} is an out-of-plane vibration of the selenium atoms. Notably, the DFT results agree within 6 cm^{-1} of the experimental values (at 300 K) with predicted frequencies for the two-phonon, E^1_{2g}, and A_{1g}, modes at 151, 211.9, and 240.7 cm^{-1}, respectively.

The CDW phase is accompanied by an emergence of unique, optically active Raman modes, which are known as amplitude or phase modes depending on their dispersion characteristics [2]. The experimental observation of amplitude modes in Raman spectroscopy enables us to understand the formation and stability of the CDW phase [6–8]. Changes in the Raman spectrum in Fig. 1 due to the CDW transition can be characterized into four categories. (1) Changes to the frequency, full width at half maximum (FWHM), and intensity of the E^1_{2g} and A_{1g} Raman phonon modes. (2) Strong, LF CDW modes appear at 42, 49, 64, and 82 cm^{-1}. (3) Peaks emerge in two clusters between 175 and 200 cm^{-1}. (4) The two-phonon mode undergoes a significant change between the metallic (300 K) and the CDW phase (5 K), indicating that it is sensitive to atomic displacements, specifically to the Ta-Ta in-plane rearrangements that constitute the core of the CDW structure. To explain the evolution of the lattice and resulting Raman spectra in the CDW phase, all mentioned categories will be detailed below, with particular care taken to assign the origin of the CDW state modes.

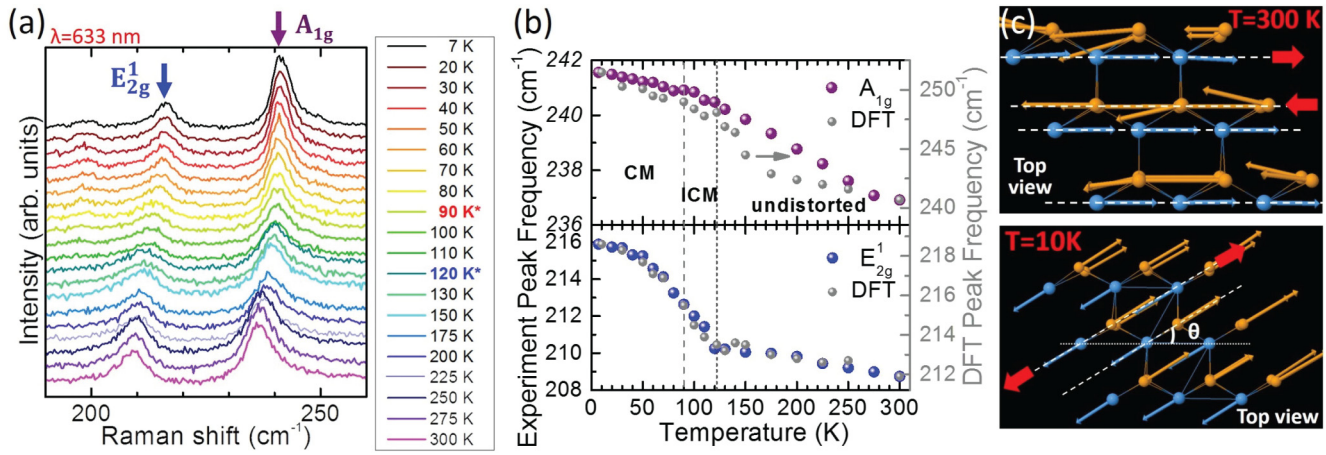

FIG. 2. (a) Normal Raman phonon spectra of $TaSe_2$ using 633-nm excitation. Transition temperatures to the incommensurate (ICM) at 122 K and commensurate (CM) at 90 K CDW states are indicated in the legend by blue and red text, respectively. (b) In the top (bottom) plot, the change in the experimental and DFT-calculated frequency of the A_{1g} (E^1_{2g}) mode is plotted as a function of temperature through the CDW transitions. Transition temperatures for the ICM- (CM-) CDW are indicated by a dark (light) gray dashed line. The A_{1g} and E^1_{2g} DFT-calculated frequencies are plotted (gray spheres) as a function of electronic temperature using the same temperature axis. (c) DFT-calculated E^1_{2g} vibrations as viewed from above for 300 and 10 K electronic temperatures. At both temperatures, all the selenium and tantalum atoms vibrate parallel to one another in the plane, but the direction of those vibrations at 10 K occurs 30° relative to the vibrations at 300 K yet remains in the plane.

The temperature dependence of the E^1_{2g} (blue) and A_{1g} (purple) modes is summarized in Fig. 2(a) and shows the Raman spectrum from 7 to 300 K excited using 1 mW of 633-nm laser light. Both the E^1_{2g} and the A_{1g} modes blueshift as temperature decreases, but the modality of the frequency shift is different between the two: the A_{1g} frequency increases (hardens), as expected by lattice anharmonic effects, by approximately 5 cm^{-1} monotonically, saturating at low temperatures, while the E^1_{2g} mode exhibits a sudden, discontinuous frequency increase at the incommensurate (ICM) CDW transition temperature. DFT results show qualitative agreement for both modes, as shown in Fig. 2(b), and even quantitative agreement can be seen for E^1_{2g} . More information on these data can be found in the SM [26].

The discontinuity of the E^1_{2g} frequency highlights that the in-plane Raman mode is sensitive to the distortion of the atomic positions in the CDW phase, which follows from the quasi-two-dimensional, in-plane nature of the CDW phase, as we will discuss. Furthermore, the sudden change in the frequency of the E^1_{2g} mode offers an experimental method to monitor the transition to the CDW state. DFT calculations show that the direction of the E^1_{2g} mode vibration rotates abruptly in plane at 100 K, which is near the ICM-CDW transition. At 300 K, this vibration is parallel to the a axis. However, below 100 K, the E^1_{2g} still vibrates in plane, but at an angle of 30° with respect to the horizontal, as seen in Fig. 2(c). This rotation can be attributed to the structural changes experienced by the system as it adopts a striped formation. More details on this structural evolution will be provided in the next section.

Overall, the experimental temperature-dependent behavior of the A_{1g} mode was expected and, furthermore, compares well with the behavior predicted by DFT. Very minor differences arose due to the changes in the a-lattice and c-lattice parameter by 1.1% and 2.3%, respectively, at an electronic temperature of 10 K in the DFT calculations. A previous experimental x-ray diffraction study reported changes in the a lattice of 1.5% and the c lattice of 4.1% [40]. Therefore, we expect that our DFT calculations regarding the out-of-plane vibrations will be less accurate due to discrepancies in the temperature dependence of the c-lattice parameter.

The differences observed in the 5 and 300 K spectrum warranted a more in-depth analysis of the temperature dependence of the two-phonon mode and its origin. The momentum needed for this two-phonon process comes from transitions between a quasiacoustic (QA) mode and a transverse optical (TO) mode [41–44]. The phonon band structure was computed for seven electronic (smearing) temperatures. For maximum interpretability, the bands were computed using a unit cell (UC, having six atoms and resulting in 18 bands) instead of the usual $3 \times 3 \times 1$ supercell. Results for a smearing temperature of 90 K are shown in Fig. 3 [39,45–48], and the results allow us to identify the location of the Kohn anomaly as near the Brillouin zone (BZ) boundary at the M point. Due to van der Waals interactions between the two $TaSe_2$ layers, the frequency at the anomaly point decreases as the temperature decreases [Fig. 3(b)], with its momentum staying constant. At temperatures below the CDW transition, the UC does not take on the correct structure due to the limited UC size. This inability to form the CDW state is evident in Fig. 3(a), where two acoustic phonon branches are negative over a large range of momentum space, indicating structural instability.

Since these inaccuracies persist in the UC computations, Fig. 3(c) displays the two-phonon mode frequencies obtained from both the supercell calculations (in blue) and the UC calculations (in black), with both calculations being compared with our experimental findings (in red). All three curves show similar trends in the stable metallic range and freeze below the CM-CDW transition (additionally, in the supercell case, there is complete stripe formation at below 60 K). Lastly, excellent agreement is found in the frequency change, or mode position,

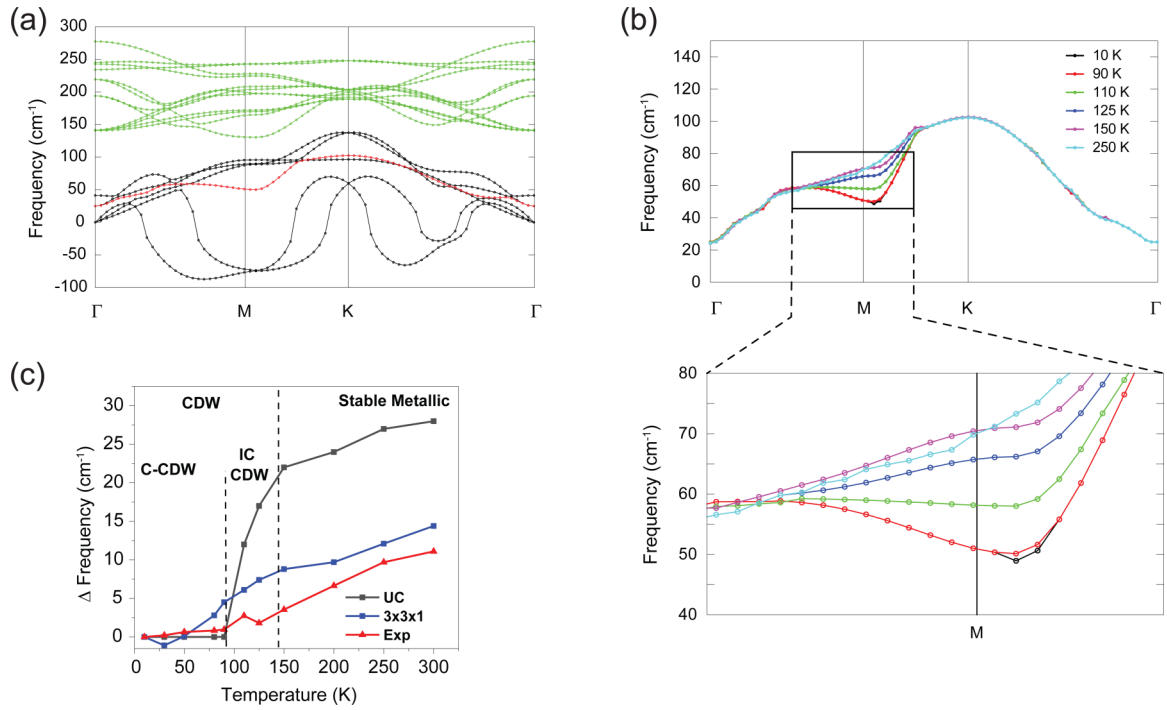

FIG. 3. (a) The calculated phonon dispersion at 90 K. Green dotted lines represent optical branches, whereas acoustic and QA modes are in black (with the exception of the one QA mode involved in the two-phonon mode that is in red). (b) Calculated evolution of the two-phonon band as a function of smearing temperature for the unit cell of 2H-$TaSe_2$. (c) UC, supercell, and experimental results for the frequency shift as a function of temperature.

of all three aforementioned cases over the full temperature range accessed experimentally. The change in slope between the metallic and the CDW phase indicates that the two-phonon mode is very sensitive to atomic displacements, specifically to the Ta-Ta in-plane rearrangements that constitute the core of the CDW structure. From the discussion above, one may conclude that the frequency shift of the two-phonon mode as a function of smearing temperature is a good indicator to identify the ICM-CDW and CM-CDW phase of $TaSe_2$, even if one only uses UC calculations.

B. Lattice evolution below the CDW transition

The excellent agreement between our DFT calculations and experiment supports the validity of the calculated structure. In Fig. 4(a), the evolution of the atomic rearrangement of $TaSe_2$ is shown as it enters the CDW state. The electronic structure is calculated as a function of electronic temperature (and smearing factor σ) in steps of 10 K. These DFT calculations reveal that the structure begins to change at a critical electronic temperature of approximately 122 K. At 90 K, the Ta atoms of the superlattice structure form a triangular structure, and Ta-rich stripes form as the temperature decreases to 30 K. Experimental indications of stripe formation were not observed in our polarization-dependent or sample-orientation-dependent measurements due to our 1-μm-laser spot measuring multiple nanometer-scale domains of different stripe orientations, thereby averaging out the stripe alignment. However, the stripes have been measured in similar systems using scanning tunneling microscopy [49–51]. In Fig. 4(b), the change in Se-Se intralayer and Se-Ta-Se interlayer distances are shown using a radial distribution function in the DFT calculations. Below the CM-CDW transition temperature, Se-Se intralayer distances start to decrease, with the shortest spacing of 3.2 Å found for Se atoms residing between the Ta stripes.

Below the ICM-CDW transition temperature of 122 K, previously unanalyzed Raman modes emerge and are shown in Fig. 5(a). Two modes observed at 196 and 172 cm^{-1} gradually appear as the temperature is reduced. Data acquired at even smaller temperature increments ($\Delta T = 2$ K increments), but a limited temperature window, are shown in Fig. 5-SM [26]. In the CM-CDW, a mode at 181 cm^{-1} and a band of modes centered around 196 cm^{-1} emerge. The observation of these peaks only below the CDW transition temperature implies that they are due to the CM-CDW. Additionally, these peaks do not have significant temperature dependence experimentally [see Fig. 5(b)], or for DFT calculations, due to the expected asymptotic behavior exhibited by phonons as they gradually freeze out with decreasing temperature. These additional midfrequency CDW peaks in $TaSe_2$ arise from Raman bands being folded to the zone center due to the new lattice periodicity, i.e., zone folding. Raman modes are predicted at 175.7 cm^{-1}, 176.6, 181.9, 194.9, and 196.4 cm^{-1}. Only the mode at 194.9 cm^{-1} appears in the ICM-CDW state, while the rest emerge in the CM-CDW state. The natures of the modes appearing in the CM-CDW state [Figs. 5(d) and 5(e)] are different than the mode which appears in the ICM-CDW state [Fig. 5(c)]. The 194.9 cm^{-1} mode consists of in-plane vibrations of Ta atoms in one direction and antiparallel vibrations of the Se atoms. In Figs. 5(d) and 5(e), we show the 176.6 cm^{-1} mode as a representative of the behavior common

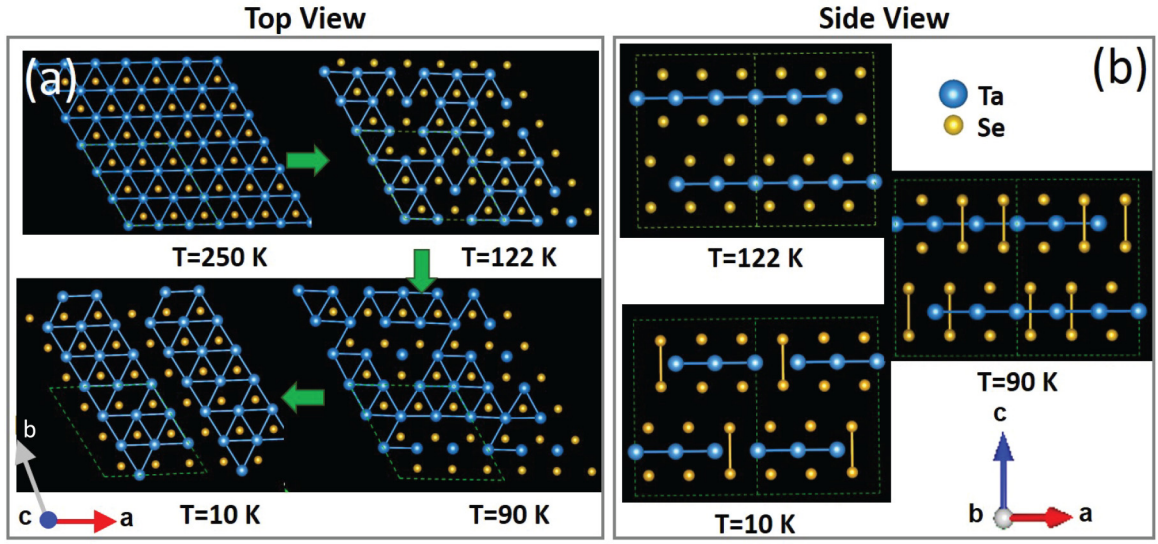

FIG. 4. (a) DFT-calculated atomic rearrangement driven by the formation of the CDW phase, viewed from above. Ta-Ta bonds (blue lines) are drawn for Ta atom separation less than 0.340 nm. The breaking of hexagonal symmetry is visible for $T = 122$ K and $T = 90$ K. The final configuration ($T = 10$ K) shows the clear formation of a 1D stripe structure for the Ta atoms. (b) Side views at select temperatures showing the gradual formation of out-of-plane Se-Se bonding within the layer; bonds are drawn for atom separation <0.325 nm. At $T = 122$ K, no Se-Se bonds are observed. However, at $T = 90$ K, Se-Se bonds begin to form at random locations within the layer. Finally, at $T = 10$ K, there are Se-Se bonds for all Se atoms between the Ta stripes and no other Se atoms.

to all the CM-CDW modes (see SM [26]). From our findings, we can conclude that circular phonon modes are a signature of the CM-CDW phase.

With decreasing temperature, four LF modes emerge experimentally: one in the ICM phase and three only in the CM phase. All emerging modes in the CM-CDW phase consist of circular vibrations of the Ta and Se atoms in opposite directions according to the DFT calculations. These in-plane and circular atomic motions indicate the broken inversion symmetry of the lattice, which was recently mentioned in the context of electron-phonon coupling in phonon-driven topological states and energy-efficient information

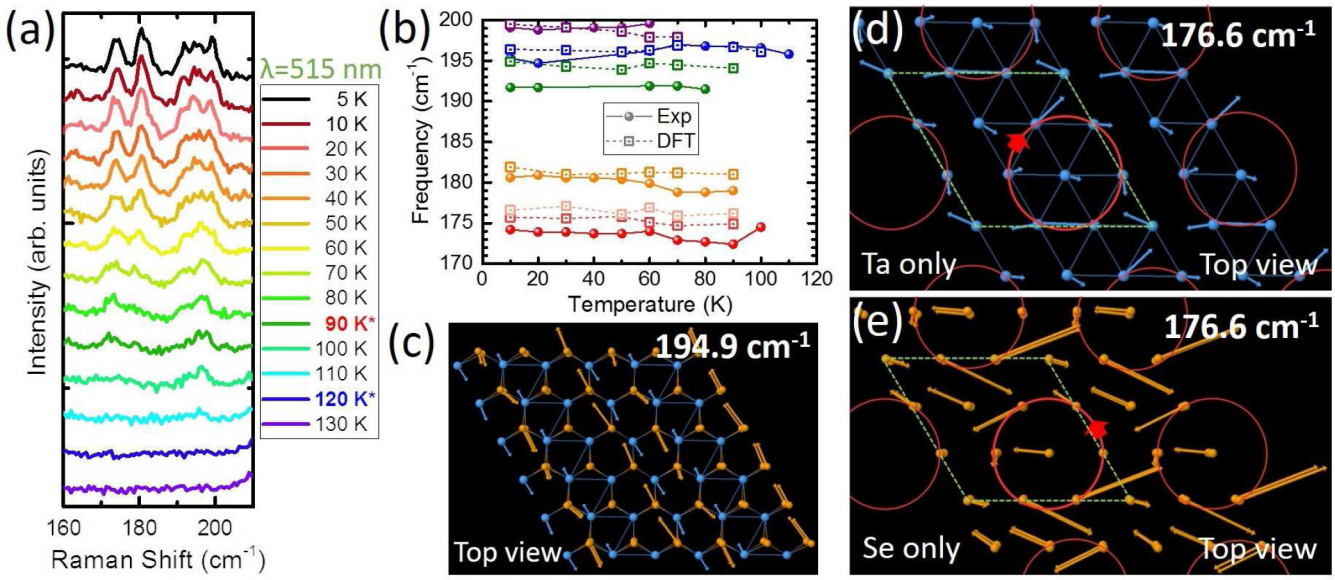

FIG. 5. (a) Raman spectra at 515-nm excitation show the emergence of modes located at 175 and 181 cm^{-1}, and a band of modes centered around 196 cm^{-1}. The transition temperature for the ICM (CM) phase is indicated in the legend by blue (red) text. (b) Comparison of experimental (solid lines) and DFT-calculated (dotted lines) frequencies in the 170–200 cm^{-1} range as a function of temperature. (c) Top view of the DFT-calculated vibrations for the mode at 194.9 cm^{-1}, which emerges in the ICM-CDW phase. (d) Top view of the DFT-calculated vibrations of the Ta and (e) Se atoms for the mode at 176.6 cm^{-1}, which emerges in the CM-CDW phase. Interestingly, both Ta and Se vibrations are in plane and circular with opposite helicities.

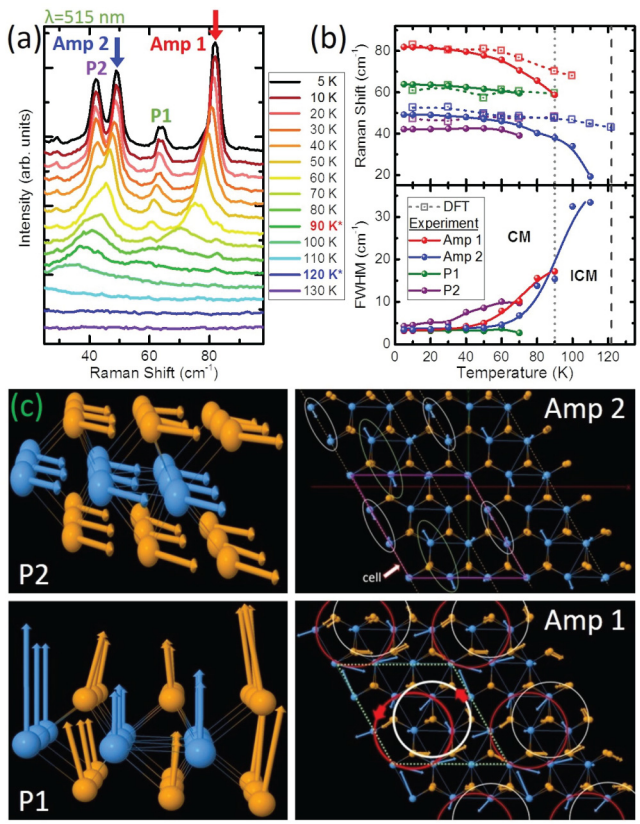

FIG. 6. (a) LF Raman spectra using 515-nm excitation. Four modes emerge at low temperatures: Amp 1, Amp 2, P1, and P2. Amp 1 and Amp 2, indicated by red and blue arrows, respectively, are the CDW amplitude modes, and P1 and P2 are the phase modes. The transition temperature for the ICM (CM) phase is indicated in the legend by the blue (red) star. (b) Temperature dependence of the frequencies and FWHM of Amp 1, Amp 2, P1, and P2. The DFT-calculated frequencies are plotted as a function of electronic temperature using the same temperature axis. Solid lines guide the eye. The transition temperature for the ICM- (CM-) CDW is indicated by a dark (light) gray dashed line. (c) DFT-calculated vibrations for the phase (side view) and amplitude (top view) modes.

processors [52]. The Raman spectra, shown for a range of temperatures below 130 K in Fig. 6(a), were measured using 515-nm excitation. The modes labeled as Amp 1 and Amp 2, at 49 and 82 cm^{-1} in the 5 K spectrum, respectively, become narrower and increase in both frequency and intensity as the temperature decreases, as seen in Fig. 6(b). DFT-calculated frequencies for these same modes are 52.5 and 87.5 cm^{-1}, at an electronic temperature (and smearing factor σ) of 10 K, which are surprisingly again within 6 cm^{-1} of the experimental data. The other two modes (P1 and P2) are the last to emerge with decreasing temperature, appearing only for temperatures lower than 70 K (or the CM-CDW state). Their frequency and intensities do not change significantly with temperature compared to Amp 1 and Amp 2 modes.

Lee *et al.* predicted the appearance of two different modes in a one-dimensional (1D) metal in a CDW state: an amplitude mode (amplitudon) and a phase mode (phason) [53]. The phase mode is a vibration representing the electron density wave in an atomic lattice which has been rearranged (as opposed to a phonon which concerns the translation of atomic positions), while the amplitude mode is a vibration of the ions resulting in an oscillation of the intensity of the maximum/minimum charge density and the magnitude of the CDW gap. The amplitude and phase modes are identified by their frequency shift, intensity, and damping rates. The narrowing and intensifying of Amp 1 and Amp 2 with decreasing temperature assigns them as amplitude modes of the CDW [6–8]. This assignment also agrees surprisingly well with the calculated band gap of 5 meV (40 cm^{-1}). The other two LF peaks, at 42 cm^{-1} (P1) and 64 cm^{-1} (P2) for $T = 5$ K, have been the subject of much debate about their assignment (see summary in Ref. [7]). As the temperature decreases, the intensity of these two modes increases more rapidly than the intensity of the amplitude modes, but otherwise the frequencies and FWHM do not vary significantly with temperature. This observation assigns these peaks as phase modes. Experimentally, the phase modes are observed only in the CM-CDW state because they have acoustic (not optical) dispersions in the ICM state and are therefore not Raman active. Upon entering the CM state, the lattice periodicity becomes three times that of the undistorted lattice, reducing the first Brillouin zone to one-third of its previous size. Therefore, the band for the acoustic Kohn anomaly folds twice, creating an optical phase mode at the zone center (see illustration in Fig. 5-SM(c) [26]). Two optical phase modes exist because the twofold degeneracy in the Kohn anomaly band is lifted when entering the CDW state.

In the right-side panels of Fig. 6(c), we show the atomic vibration of the two amplitude modes at an electronic temperature of 10 K. The Ta and Se atoms of Amp 1 vibrate in plane, in a circular motion around three hexagons of the original lattice, with all the vibrations having one helicity within a stripe. For Amp 2, Ta atoms oscillate in plane along the direction of the stripe in two of the three rows that form the stripes, whereas the Se atoms vibrate in the out-of-plane direction. Note that the apparent lack of vibrations in the third row of Ta is likely a product of the periodic boundary conditions, namely, that the third row cannot vibrate while maintaining the supercell boundary conditions. The vibrations of P1 and P2 are simpler. P2 is an in-plane vibration of all atoms in the same direction as, and roughly orthogonal to, the stripe, whereas P1 is an out-of-plane vibration of all atoms in the same direction. Both of these phase vibrations lead to an expected oscillation of the phase of the CDW [2].

IV. CONCLUSIONS

In conclusion, temperature-dependent Raman spectra from 2H-$TaSe_2$ were collected at temperatures ranging from 5 to 300 K. An abrupt blueshift of the E^1_{2g} phonon was observed when the material entered the ICM-CDW state upon cooling from the undistorted state, unlike the gradual, continuous blueshift of the A_{1g} mode. The E^1_{2g} mode couples more strongly to the CDW state confirming the CDW is an in-plane distortion. DFT results replicated this behavior, revealing that in the CDW state, the E^1_{2g} vibrational direction rotates by 30° in the plane. The frequency and FWHM of the LF

CDW modes were identified and assigned as amplitude or phase modes. Additionally, zone-folded CDW modes emerge due to changes in the lattice periodicity. DFT calculations also indicated that the atomic displacements associated with the CDW form a 1D Ta-rich stripe structure, a phenomenon unique to the commensurate CDW phase. With these phonon origins clarified, a template for understanding the relationship between Raman spectra and atomic displacement in CDW states of layered materials has been developed. Our findings identify Raman spectroscopy as an extremely well-suited technique to investigate atomic modifications within a charge density wave when coupled with validated theoretical models.

ACKNOWLEDGMENTS

H.M.H. and A.F.R. would like to thank the National Research Council's Research Associateship Program.

Commercial equipment, instruments, and materials are identified in this paper in order to specify the experimental procedure adequately. Such identification is not intended to imply recommendation or endorsement by the National Institute of Standards and Technology or the United States government, nor is it intended to imply that the materials or equipment identified are necessarily the best available for the purpose.

The authors declare no competing interests.

[1] G. Liu, B. Debnath, T. R. Pope, T. T. Salguero, R. K. Lake, and A. A. Baladin, Nat. Nanotechnol. **11**, 845 (2016).
[2] G. Gruner, *Density Waves in Solids* (Perseus Publishing, New York, 2000).
[3] J. A. Wilson, F. J. Di Salvo, and S. Mahajan, Adv. Phys. **24**, 117 (1975).
[4] J. A. Wilson and A. D. Yoffe, Adv. Phys. **18**, 193 (1969).
[5] B. Sipos, A. F. Kusmartseva, A. Akrap, H. Berger, L. Forró, and E. Tutis, Nat. Mater. **7**, 960 (2008).
[6] E. F. Steigmeier, G. Harbeke, H. Auderset, and F. J. DiSalvo, Solid State Commun. **20**, 667 (1976).
[7] J. C. Tsang, J. E. Smith, Jr., and M. W. Shafer, Phys. Rev. B **16**, 4239 (1977).
[8] S. Sugai, K. Murase, S. Uchida, and S. Tanaka, J. Phys., Colloq. **42**, C6-728 (1981).
[9] J. A. Wilson, F. J. DiSalvo, and S. Mahajan, Phys. Rev. Lett. **32**, 882 (1974).
[10] T. M. Rice and G. K. Scott, Phys. Rev. Lett. **35**, 120 (1975).
[11] M. D. Johannes, I. I. Mazin, and C. A. Howells, Phys. Rev. B **73**, 205102 (2006).
[12] A. H. Castro Neto, Phys. Rev. Lett. **86**, 4382 (2001).
[13] W. L. McMillan, Phys. Rev. B **14**, 1496 (1976).
[14] M. D. Johannes and I. I. Mazin, Phys. Rev. B **77**, 165135 (2008).
[15] S. Sugai and K. Murase, Phys. Rev. B **25**, 2418 (1982).
[16] D. E. Moncton, J. D. Axe, and F. J. DiSalvo, Phys. Rev. Lett. **34**, 734 (1975).
[17] J. A. Holy, M. V. Klein, W. L. McMillan, and S. F. Meyer, Phys. Rev. Lett. **37**, 1145 (1976).
[18] J. C. Tsang, J. E. Smith, Jr., and M. W. Shafer, Solid State Commun. **27**, 145 (1978).
[19] J. A. Wilson, Phys. Rev. B **17**, 3880 (1978).
[20] P. Hajiyev, C. Cong, C. Qiu, and T. Yu, Sci. Rep. **3**, 2593 (2013).
[21] K. Rossnagel, E. Rotenberg, H. Koh, N. V. Smith, and L. Kipp, Phys. Rev. B **72**, 121103(R) (2005).
[22] K. Rossnagel and N. V. Smith, Phys. Rev. B **76**, 073102 (2007).
[23] S. V. Borisenko, A. A. Kordyuk, A. N. Yaresko, V. B. Zabolotnyy, D. S. Inosov, R. Schuster, B. Büchner, R. Weber, R. Follath, L. Patthey, and H. Berger, Phys. Rev. Lett. **100**, 196402 (2008).
[24] P. Manchanda, V. Sharma, H. Yu, D. J. Sellmyer, and R. Skomski, Appl. Phys. Lett. **107**, 032402 (2015).
[25] R. Samnakay, D. Wickramaratne, T. R. Pope, R. K. Lake, T. T. Salguero, and A. A. Balandin, Nano Lett. **15**, 2965 (2015).
[26] See Supplemental Material at http://link.aps.org/supplemental/10.1103/PhysRevB.99.174110 for Raman modes with different excitation wavelengths, temperature dependence of Raman modes using 515-nm excitation, temperature dependence of the charge density wave modes using 633-nm excitation, cross- and parallel-polarized Raman spectra, temperature dependence of higher-frequency Raman modes, and computational methods. Also see Refs. [27–36].
[27] J. P. Perdew and Y. Wang, Phys. Rev. B **45**, 13244 (1992).
[28] J. P. Perdew, J. A. Chevary, S. H. Vosko, K. A. Jackson, M. R. Pederson, D. J. Singh, and C. Fiolhais, Phys. Rev. B **46**, 6671 (1992).
[29] J.-A. Yan, M. A. D. Cruz, B. Cook, and K. Varga, Sci. Rep. **5**, 16646 (2015).
[30] N. D. Mermin, Phys. Rev. **137**, A1441 (1965).
[31] W. Kohn, Phys. Rev. Lett. **2**, 393 (1959).
[32] D. L. Duong, M. Burghard, and J. C. Schön, Phys. Rev. B **92**, 245131 (2015).
[33] M. Calandra, I. I. Mazin, and F. Mauri, Phys. Rev. B **80**, 241108(R) (2009).
[34] F. Weber, S. Rosenkranz, J.-P. Castellan, R. Osborn, R. Hott, R. Heid, K.-P. Bohnen, T. Egami, A. H. Said, and D. Reznik, Phys. Rev. Lett. **107**, 107403 (2011).
[35] K. Motizuki, N. Suzuki, Y. Yoshida, and Y. Takaoka, Solid State Commun. **40**, 995 (1981).
[36] Y. Ge and A. Y. Liu, Phys. Rev. B **86**, 104101 (2012).
[37] P. Giannozzi, S. Baroni, N. Bonini, M. Calandra, R. Car, C. Cavazzoni, D. Ceresoli, G. L. Chiarotti, M. Cococcioni, and I. Dabo, J. Phys.: Condens. Matter **21**, 395502 (2009).
[38] S. Sugai, Phys. B (Amsterdam, Neth.) **117-118**, 587 (1983).
[39] M. V. Klein, Phys. Rev. B **24**, 4208 (1981).
[40] J. L. Feldman, C. L. Vold, E. F. Skelton, S. C. Yu, and I. L. Spain, Phys. Rev. B **18**, 5820 (1978).
[41] B. Chakraborty, H. R. Matte, A. Sood, and C. Rao, J. Raman Spectrosc. **44**, 92 (2013).
[42] T. Livneh and J. E. Spanier, 2D Mater. **2**, 035003 (2015).
[43] B. R. Carvalho, Y. Wang, S. Mignuzzi, D. Roy, M. Terrones, C. Fantini, V. H. Crespi, L. M. Malard, and M. A. Pimenta, Nat. Commun. **8**, 14670 (2017).

[44] T. Sekine, K. Uchinokura, T. Nakashizu, E. Matsuura, and R. Yoshizaki, J. Phys. Soc. Jpn. **53**, 811 (1984).
[45] A. Kawabata, J. Phys. Soc. Jpn. **30**, 68 (1971).
[46] P. Venezuela, M. Lazzeri, and F. Mauri, Phys. Rev. B **84**, 035433 (2011).
[47] K. Motizuki, K. Kimura, and N. Suzuki, J. Phys. Soc. Jpn. **53**, 1078 (1984).
[48] T. Nakashizu, T. Sekine, K. Uchinokura, and E. Matsuura, J. Phys. Soc. Jpn. **55**, 672 (1984).
[49] J. Wang, H. Zheng, G. Xu, L. Sun, D. Hu, Z. Lu, L. Liu, J. Zheng, C. Tao, and L. Jiao, J. Am. Chem. Soc. **138**, 16216 (2016).
[50] H. Zheng, S. Valtierra, N. Ofori-Opoku, C. Chen, L. Sun, S. Yuan, L. Jiao, K. H. Bevan, and C. Tao, Nano Lett. **18**, 2179 (2018).
[51] A. Soumyanarayanan, M. M. Yee, Y. He, J. van Wezel, D. J. Rahn, K. Rossnagel, E. W. Hudson, M. R. Norman, and J. E. Hoffman, Proc. Natl. Acad. Sci. U. S. A. **110**, 1623 (2013).
[52] H. Zhu, J. Yi, M.-Y. Li, J. Xiao, L. Zhang, C.-W. Yang, R. A. Kaindl, L.-J. Li, Y. Wang, and X. Zhang, Science **359**, 579 (2018).
[53] P. A. Lee, T. M. Rice, and P. W. Anderson, Solid State Commun. **14**, 703 (1974).